THE JOURNAL OF PHYSICAL CHEMISTRY A

Article

pubs.acs.org/JPCA

Refined Representation of Falloff Curves for the Reaction HO + NO_2 + N_2 → ($HONO_2$, HOONO) + N_2

Jürgen Troe

Institut für Physikalische Chemie der Universität and Max-Planck-Institut für Biophysikalische Chemie, Göttingen Tammannstrasse 6, D-37077 Göttingen, Germany

ABSTRACT: Experimental data for the reactions (1) HO + NO_2 (+N_2) → $HONO_2$ (+N_2) and (2) HO + NO_2 (+N_2) → HOONO (+N_2) near 300 K and over the pressure range 1 Torr to 320 bar are represented in terms of novel asymmetric broadening factors in falloff expressions. This analysis allows for a refined representation of the data, reproducing fine details of $k = k_1 + k_2$ and k_2/k_1 and probably allows for a better extrapolation to the limiting low and high pressure rate constants than possible with symmetric broadening factors in conventional falloff expressions. The experimental data clearly show that the center broadening factor $F_{cent,1}$ is close to 0.41 and consistent with results from theoretical modeling. This value of F_{cent} markedly differs from the "standard value" of 0.6, and the consequences of this difference are illustrated. Limiting rate constants of $k_{1,0} = [N_2]\ (T/300\ K)^{-4.5}\ 3.2 \times 10^{-30}$ cm^6 molecule^{-2} s^{-1}, $k_{2,0} = [N_2]\ (T/300\ K)^{-4.5}\ 1.0 \times 10^{-31}$ cm^6 molecule^{-2} s^{-1}, $k_{1,\infty} = 2.7 \times 10^{-11}$ cm^3 molecule^{-1} s^{-1}, and $k_{2,\infty} = 4.8 \times 10^{-11}$ cm^3 molecule^{-1} s^{-1} are obtained and tested over the range 220−300 K, whereas the exponent −4.5 changes to −3.0 in $k_{1,0}$ and $k_{2,0}$ over the range 300−430 K (the values correspond to falloff curves with asymmetric broadening factors).

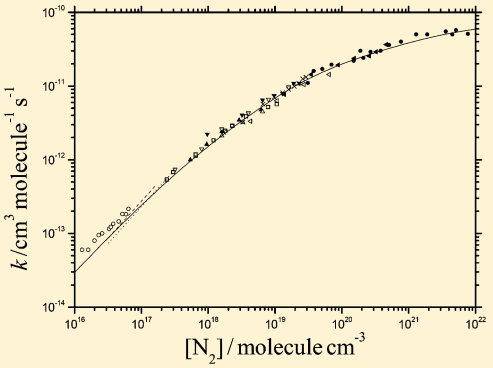

1. INTRODUCTION

The association reaction of hydroxyl radicals with nitrogen dioxide forming nitric acid,

$$HO + NO_2(+M) \rightarrow HONO_2(+M)\ (k_1) \quad (1.1)$$

and peroxynitrous acid,

$$HO + NO_2(+M) \rightarrow HOONO(+M)\ (k_2) \quad (1.2)$$

is the single most important radical sink in atmospheric chemistry. For this reason, there have been numerous experimental and theoretical studies determining and analyzing the rate constants k_1 and k_2; see, e.g., the NASA/JPL[1] and IUPAC[2] evaluations. To incorporate these data into large scale models of atmospheric kinetics and photochemistry, suitable expressions for the dependence of the rate constants on the bath gas concentration [M] (or the bath gas pressure P) and the temperature T are required. This is the issue of the present article, which intends to derive a refined representation of the pseudo-second-order rate constants k_1 and k_2 as functions of [M] and T.

There are a variety of options to represent single-channel rate constants $k([M],T)$ in the falloff range between the limiting low pressure rate constants k_0 and the limiting high pressure rate constants k_∞. In the early 1970s, using the reaction between HO and NO_2 as an example, attempts were made to express the pressure dependence of k by a polynomial in P. To have a physically more logical approach, the present author in 1979, and for the recombination of OH with NO_2, suggested[3] the use of doubly reduced representations of k/k_∞ as a function of a "reduced pressure scale"

$$x = k_0/k_\infty \quad (1.3)$$

(with k_0 being proportional to [M]). Starting from the only qualitatively correct Lindemann−Hinshelwood expression,

$$(k/k_\infty)_{LH} = x/(1 + x) \quad (1.4)$$

broadening factors $F(x)$ were introduced through

$$k/k_\infty = [x/(1 + x)]F(x) = (k/k_\infty)_{LH}F(x) \quad (1.5)$$

The analysis of rigid activated complex, strong collision, RRKM (Rice−Ramsperger−Kassel−Marcus) calculations led to an approximate relationship for strong collision broadening factors $F^{sc}(x)$,

$$F^{sc}(x) \approx (F^{sc}_{cent})^{1/[1+(\log x/N)^2]} \quad (1.6)$$

with

$$N \approx 0.75 - 1.27 \log F^{sc}_{cent} \quad (1.7)$$

Special Issue: A. R. Ravishankara Festschrift

Received: December 15, 2011
Revised: January 19, 2012
Published: January 24, 2012

   dx.doi.org/10.1021/jp212095n | J. Phys. Chem. A 2012, 116, 6387−6393

and F_{cent}^{sc} being the value of $F^{sc}(x)$ at the "center of the falloff curve", i.e., at $x = 1$. Weak collision effects in addition were accounted for by generalizing eq 1.5 to

$$F(x) = F^{sc}(x)\, F^{wc}(x) \tag{1.8}$$

with $F^{wc}(x)$ given by an expression analogous to eq 1.6. Representative solutions of the master equation resulted in a relation between F_{cent}^{wc}, defined by $F_{cent}^{wc} = F^{wc}(x{=}1)$, and the collision efficiency β_c, contained in k_0, of the tentative form

$$F_{cent}^{wc} \approx \beta_c^{\,0.14} \tag{1.9}$$

It was clear that eqs 1.3−1.9 were only approximate and should be tested against more rigorous theory and also be tested in practical applications. In particular, refinements will be made using asymmetric broadening factors (i.e., $F(x) \neq F(-x)$) instead of the symmetric broadening factors (i.e., $F(x) = F(-x)$) like eq 1.6.

Equations 1.3−1.8 have become standard; see, e.g., the NASA/JPL[1] and IUPAC[2] databases. However, two different strategies were followed. To minimize the number of parameters required for data representation, the actual NASA/JPL evaluations[1] express k_0 and k_∞ in the form

$$k_0 = [\mathrm{M}]k_0^{300}(T/300\ \mathrm{K})^{-n} \tag{1.10}$$

and

$$k_\infty = k_\infty^{300}(T/300\ \mathrm{K})^{-m} \tag{1.11}$$

and then fix $F_{cent} = F_{cent}^{sc}F_{cent}^{wc}$ to a "standard value" of

$$F_{cent} \approx 0.6 \tag{1.12}$$

which through eq 1.7 leads to $N \approx 1$ in eq 1.6. Following this concept, the parameters k_0^{300}, n, k_∞^{300}, and m are tabulated. The actual IUPAC evaluations,[2] in most cases, instead use the parameters k_0^{300}, n, k_∞^{300}, and F_{cent}, while assuming k_∞ and F_{cent} to be only weakly temperature dependent. Both policies thus require four parameters for representing the pressure and temperature dependences of k. Obviously, the two policies can only be approximate and valid only over limited ranges of conditions. However, both strategies have been proven useful in reproducing experimental data equally well, at least over limited parts of the falloff curve.

Although the two approaches to the problem both have their merits, it appears necessary to check their respective performances for systems where the experimental database is sufficiently large and/or realistic theoretical calculations are available as well. Reactions 1.1 and 1.2 again provide this opportunity. There are a number of experimental studies at pressures in the Torr range approaching the low pressure limit. On the other hand, there are experiments at bath gas pressures up to several hundred bar approaching the high pressure limit. There appeared to be a problem with data in the intermediate part of the falloff curve at pressures near 1 bar. Here, differences between the results from several laboratories up to a factor of 2 were observed. Because this range is of particular importance for tropospheric photochemistry, the situation appeared unsatisfactory. However, in the meantime new experiments have been performed with particular care to minimize experimental uncertainties.[4] These experiments suggest that some of the earlier data should be discarded, leaving an uncertainty of only 10−20% of the room temperature rate constant near one bar. In addition, direct information on the branching ratio k_2/k_1 and its pressure and temperature dependence has been obtained[4,5] such that the two processes can also be separated.

Besides the pressure dependence also the temperature dependence has been studied extensively, mostly over the range 220 to about 600 K. The temperature range can be further extended by including experimental studies of the thermal dissociation of nitric acid,[6−8] i.e., the reverse of reaction 1.1. Likewise, experimental information on the dissociation of peroxynitrous acid, i.e., the reverse of reaction 1.2, has become available.[5,9] Finally, because high pressure rate constants of reaction 1.1 are related to measurements of the vibrational relaxation of hydroxyl radicals in collisions with nitrogen dioxide, experimental studies[10,11] of the process

$$\mathrm{HO}(v{=}1) + \mathrm{NO_2} \rightarrow \mathrm{HO}(v{=}0) + \mathrm{NO_2} \qquad (k_{13}) \tag{1.13}$$

are also relevant for the analysis of the system.

The performance of eqs 1.3−1.9 can be tested by comparison with the experimental data. At the same time, these equations are used for extrapolations of the experiments to the limiting rate constants k_0 and k_∞. On the other hand, these equations have to be controlled by theoretical calculations using unimolecular rate theory. Although a series of such calculations have been performed for reactions 1.1 and 1.2 (see, e.g., refs 9 and 12−19), the various approaches all still leave something to desire; see below. Therefore, testing eqs 1.3−1.8 against theories specifically devoted to reactions 1.1 and 1.2 appears not sufficient. Instead, more general studies of strong collision falloff curves for dissociation and recombination reactions[20−22] should be consulted as well, to refine eqs 1.3−1.8. Furthermore, new studies of weak collision broadening factors[22] allow one to test eqs 1.8 and 1.9. By combining the still fragmentary experiments with the likewise only semiquantitative theoretical models, in spite of the remaining problems, it appears possible now to assess the quality of the data representations, and to judge the possibilities for extrapolating rate data outside the studied range of conditions. This is the aim of the present article.

2. SIMPLIFIED REPRESENTATION OF THE FALLOFF CURVE $k([\mathrm{M}])$ AT 300 K

We start with the (now outdated, see below) assumption that there is a single reaction channel 1.1 only and we proceed to an experimental determination of the center broadening factor F_{cent} and of the location $[\mathrm{N_2}]_{cent}$ of the center of the falloff curve at which

$$k_0([\mathrm{N_2}]) = k_\infty \tag{2.1}$$

(corresponding to $x = 1$, or $[\mathrm{N_2}]_{cent} = k_\infty/k_0$). We consider experimental data measured at the lowest and highest available pressures (and we slightly extrapolate them to the limiting low and high pressure ranges). Instead of relying on eqs 1.3−1.8, we use the optimum novel representation of falloff curves derived in ref 22. By systematic variation of molecular parameters, this work showed that there is no unique falloff representation, each reaction system showing a specific shape of $F(x)$. However, for the same F_{cent}, the individual broadening factors $F(x)$ all fell into a narrow band of values spread around

dx.doi.org/10.1021/jp212095n | J. Phys. Chem. A 2012, 116, 6387−6393

a central curve, which could well be fitted by an expression of the form

$$F(x) \approx 1 - (1 - F_{cent}) \exp\{-[\log(1.5x)/N]^2/N^*\} \quad (2.2)$$

where $N = 0.75 - 1.27 \log F_{cent}$ as in eq 1.7, $N^* = 2$ for $\log(1.5x) > 0$, and $N^* = 2[1 - 0.15 \log(1.5x)]$ for $\log(1.5x) < 0$. Equation 2.2 corresponds to an asymmetric broadening factor (i.e., $F(x) \neq F(-x)$) in contrast to the symmetric broadening factor of eq 1.6. Individual systems showed deviations from eq 2.2, at some values of x up to 10%, but these deviations were rare and generally the width of the band of calculated $F(x)$ was smaller. The calculations leading to eq 2.2 went beyond RRKM calculations by accounting for rotational effects, specific anisotropies of the potential, various numbers of transitional modes, and weak collision energy transfer. As theoretical calculations on the same level, for the specific reaction systems 1.1 and 1.2, have not yet been performed in the available theoretical work, we follow the general approach of ref 22 and use eq 2.2, keeping in mind that unusual behavior is improbable but cannot be ruled out. We furthermore take into account the result of ref 22 that F_{cent}^{wc} decreases with decreasing β_c until it levels off at a minimum value of about 0.65.

The determination of F_{cent} from the experiments proceeds in two steps. At first, experimental values of k near to the low and high pressure limiting values are chosen, which lead to a first approximation of $[N_2]_{cent}$. Comparing experimental $k([N_2] \approx [N_2]_{cent})$ with eqs 1.3−1.8 then leads to a first approximation for F_{cent}. We note again that k in the present work denotes the sum of k_1 and k_2, i.e.

$$k = k_1 + k_2 \quad (2.3)$$

Using eq 2.2 for a fine-tuning of the extrapolation to the most probable true k_0 and k_∞, improves the derived $[N_2]_{cent}$ and from that the experimental value of F_{cent}. Finally, the complete experimental falloff curve is compared with the theoretical expression of eqs 1.3−1.8 or eq 2.2 instead of eqs 1.6−1.8.

A summary of low pressure experiments, at N_2 pressures down to 0.4 Torr, was given in refs 1 and 2, suggesting that k_0 is close to $k_0 \approx [N_2]\ 3.0 \times 10^{-30}$ cm^6 molecule^{-2} s^{-1}. The data all needed only mild extrapolations toward k_0. As shown later, the improved extrapolation with eq 2.2 does not change this value too much, which, therefore, within the given accuracy (of about ±30% estimated in ref 2) is believed to be close to the true k_0. k_{13} in ref 10 was measured as 4.8×10^{-11} cm^3 molecule^{-1} s^{-1} whereas ref 11 led to $k_{13} = 6.4 \times 10^{-11}$ cm^3 molecule^{-1} s^{-1}. The most precise high pressure measurement of k for M = He from ref 9, at pressures up to 500 bar, led to values of k_∞ in the range $(5.0-5.7) \times 10^{-11}$ cm^3 molecule^{-1} s^{-1}. Averaging these data, would suggest k_∞ to be close to $k_\infty \approx 5.5 \times 10^{-11}$ cm^3 molecule^{-1} s^{-1}. The given values of k_0 and k_∞, to a first approximation, with eq 2.1 then locate the center of the falloff curve near

$$[N_2]_{cent} = k_\infty/k_0 \approx 2.1 \times 10^{19} \text{ molecule cm}^{-3} \quad (2.4)$$

corresponding to 660 Torr at 300 K. On the basis of the experiments from refs 4, 11, and 23 near 1 bar, one then may rely on $k([N_2] = [N_2]_{cent}) \approx 1.14 \times 10^{-11}$ (ref 23), 1.15×10^{-11} (ref 11), and 1.09×10^{-11} cm^3 molecule^{-1} s^{-1} (ref 4), giving an average of $k([N_2] = [N_2]_{cent}) \approx 1.13 \times 10^{-11}$ cm^3 molecule^{-1} s^{-1}. With eq 1.5, this leads to an experimental value of

$$F_{cent} = 0.41 \quad (2.5)$$

Further fine-tuning the representation of the experimental falloff curve by eq 2.2 does not change this value anymore, see below.

On the basis of the experimental $F_{cent} = 0.41$, we proceed to a comparison of the representation of the falloff curve based on eq 2.2 with the experimental falloff curve in Figure 1. There

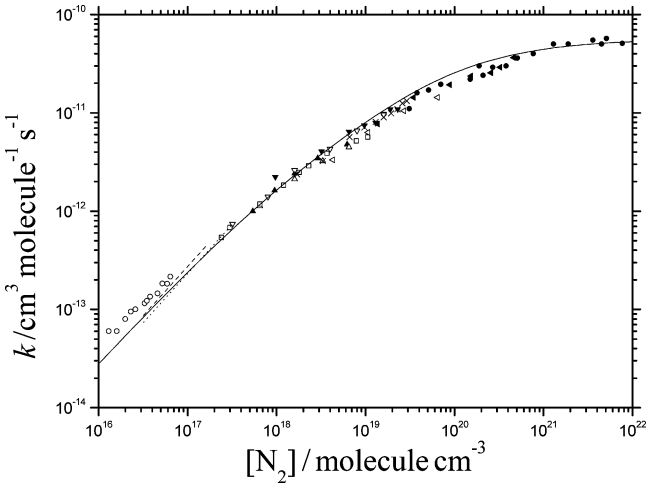

Figure 1. Comparison of experimental data for $k = k_1 + k_2$ with single-channel modeling for k (T = 298 K; full line = modeling with asymmetric falloff broadening factor of eq 2.2 using the parameters $k_0 = [N_2]\ 3.0 \times 10^{-30}$ cm^6 molecule^{-2} s^{-1}, $k_\infty = 5.5 \times 10^{-11}$ cm^3 molecule^{-1} s^{-1}, and $F_{cent} = 0.41$; experimental data points from ref 9 (●, converted from experiments with M = He), ref 24 (◀, converted from experiments with M = CF_4), ref 24 (◁, converted from experiments with M = Ar), ref 4 (×), ref 11 (▼), ref 23 (▽), ref 26 (□), ref 30 (△), ref 25 (▲), ref 27 (○), ref 28 (...), and ref 29 (---); see text).

appears to be quite satisfactory agreement over the full pressure range, from about 1 Torr up to about 320 bar. However, a few details should be noted. Following ref 9, the data from the high pressure experiments in He have been shifted by the factor of $k_{0,He}/k_{0,N_2} \approx 0.64$ toward the left such that 500 bar in He from ref 9 corresponds to 320 bar in N_2. Likewise, the experiments from ref 24 up to 4 bar in M = Ar and 8.6 bar in CF_4 are included by shifting their pressure scale by the factors $k_{0,Ar}/k_{0,N_2} \approx 0.65$[25] and $k_{0,CF_4}/k_{0,N_2} \approx 2.15$.[24,25] Obviously not all but only a representative selection of measured points could be shown in Figure 1. In particular, only top grade points (such as indicated by the authors) from ref 26 were used; when this was done, some of the discomforting discrepancies of results for 1 bar between the experiments from refs 4, 11, and 23 on the one hand, and ref 26 on the other hand, disappear. The data at the lowest pressures from ref 27 appear high and show an unusually large intercept of $k([M])$ for $[M] \rightarrow 0$, which possibly is due to wall effects. These data, therefore, are excluded and only the average of the data from refs 28 and 29 is employed to fix k_0.

Although the general agreement between the experimental points shown in Figure 1 and the representation by eqs 1.3−1.5 and 2.2, with the parameters $k_0 = [N_2]\ 3.0 \times 10^{-30}$ cm^6 molecule^{-2} s^{-1}, $k_\infty = 5.5 \times 10^{-11}$ cm^3 molecule^{-1} s^{-1}, and $F_{cent} = 0.41$, appears quite acceptable, the experimental points in the

dx.doi.org/10.1021/jp212095n | J. Phys. Chem. A 2012, 116, 6387−6393

range $10^{19} < [N_2] < 10^{21}$ molecule cm^{-3} systematically appear to be slightly lower than the representation. In the following section this is attributed to the fact that k is the sum of k_1 and k_2. Although k_1 and k_2 individually can be represented by eqs 1.3−1.8 and 2.2, their sum does not exactly follow these expressions.

Before going into the finer details, in Figure 2 we also compare the experimental data shown in Figure 1 with the

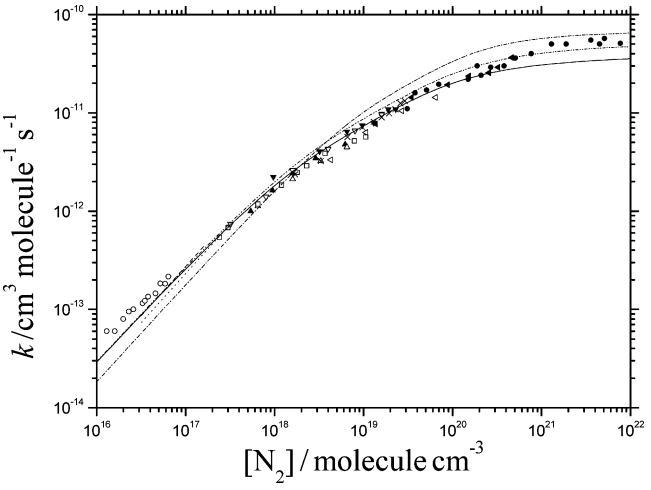

Figure 2. Comparison of experimental data for $k = k_1 + k_2$ with single-channel modeling for k (T = 298 K; experimental data as in Figure 1; modeling using eqs 1.3−1.8; full line = IUPAC representation of ref 2 with F_{cent} = 0.41, $k_0 = [N_2]$ 3.3 × 10^{-30} cm^6 molecule^{-2} s^{-1}, and k_∞ = 4.1 × 10^{-11} cm^3 molecule^{-1} s^{-1}; dot-dot-dashed line = this work with F_{cent} = 0.41, $k_0 = [N_2]$ 3.3 × 10^{-30} cm^6 molecule^{-1} s^{-1}, and k_∞ = 5.5 × 10^{-11} cm^3 molecule^{-1} s^{-1}; dash-dotted line = NASA/JPL representation of ref 1 with F_{cent} = 0.6, $k_0 = [N_2]$ 1.9 × 10^{30} cm^6 molecule^{-2} s^{-1}, and k_∞ = 7.0 × 10^{-11} cm^3 molecule^{-1} s^{-1}; see text).

NASA/JPL[1] and IUPAC[2] representations using eqs 1.3−1.8 (with the parameters $k_0 = [N_2]$ 1.9 × 10^{-30} cm^6 molecule^{-2} s^{-1}, k_∞ = 7.0 × 10^{-11} cm^3 molecule^{-1} s^{-1}, and F_{cent} = 0.6 for the NASA/JPL representation vs $k_0 = [N_2]$ 3.3 × 10^{-30} cm^6 molecule^{-2} s^{-1}, k_∞ = 4.1 × 10^{-11} cm^3 molecule^{-1} s^{-1}, and F_c = 0.4 for the IUPAC representation; for the representation in Figure 2, the separated parameters for reactions 1.1 and 1.2 of the last NASA/JPL evaluation have been added). Although the general agreement with the data at least in limited pressure ranges is not too bad, the NASA/JPL falloff representation appears "too narrow"; i.e., a too large value of F_{cent} results in too small fitted values of k_0 or k_∞. The IUPAC representation, although avoiding this problem, appears "too symmetric", showing too slow an approach to k_∞. Further considerations of these points are postponed until k_1 and k_2 are represented individually in section 3.

3. REPRESENTATION OF FALLOFF CURVES FOR $k_1([M])$ AND $k_2([M])$ AT 300 K

The preliminary analysis of the falloff curve at 300 K given in section 2 assumed that the sum of the two falloff curves for reactions 1.1 and 1.2 can be represented by the same expression as a falloff curve for a single-channel system. This need not be the case. In the present section we try to obtain individual representations of $k_1([M])$ and $k_2([M])$ and we then inspect the shape of the sum $k = k_1 + k_2$.

A construction of separate falloff curves for the two channels now can be attempted on the basis of measurements of the branching ratio k_2/k_1 at 298 K in M = N_2 over the pressure range 98−762 Torr from ref 4. With decreasing pressure, here the ratio $\alpha = k_2/k_1$ decreases from values near 0.15 to values near 0.075, such as illustrated in Figure 3. Together with other

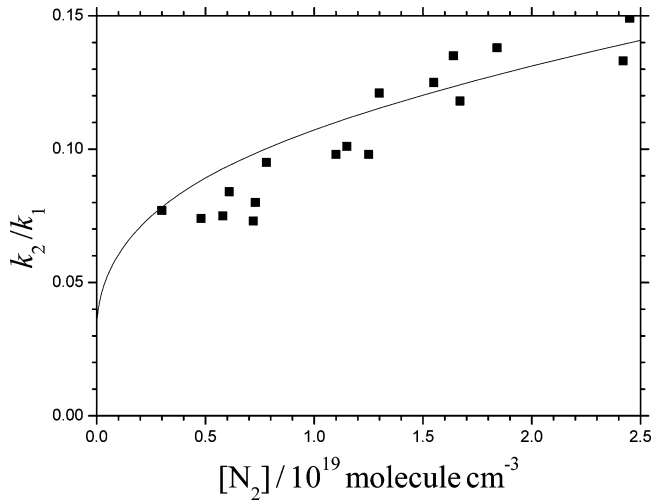

Figure 3. Comparison of experimental data for k_2/k_1 with k_2/k_1 from single-channel modelings for k_1 and k_2 (T = 298 K; full line = modeling with asymmetric falloff broadening factors of eq 2.2 using the parameters $F_{cent,1} = F_{cent,2}$ = 0.41, $k_{1,0} = [N_2]$ 3.2 × 10^{-30} cm^6 molecule^{-2} s^{-1}, $k_{2,0} = [N_2]$ 1.0 × 10^{-31} cm^6 molecule^{-2} s^{-1}, $k_{1,\infty}$ = 2.7 × 10^{-11} cm^3 molecule^{-1} s^{-1}, and $k_{2,\infty}$ = 4.8 × 10^{-11} cm^3 molecule^{-1} s^{-1}; full squares = experimental points from ref 4).

experiments[5,31−33] this suggests a low pressure limiting ratio of $k_{2,0}/k_{1,0} \approx 0.04$ (±0.01). Though this well characterizes the low pressure range, the situation is less satisfactory at the high pressure side. Values of α at pressures up to 100 bar in M = He have been obtained at 430 K in ref 5. However, these data only to a limited extent allow for an extrapolation to the high pressure limit at 298 K. On the other hand, theoretical models[9,16−19] suggest the limiting high pressure value of α to be of the order of 1.0 (±0.4). Combining these data similar to the procedure described in section 2, for reaction 1.2 this leads to $[N_2]_{cent,2} \approx 2.4 \times 10^{20}$ molecule cm^{-3} (corresponding to 7360 Torr at 298 K, such that the experiments of ref 4 with 762 Torr only reach up to $k_{2,0}/k_{2,\infty} = x_2 \approx 0.14$). This is too far away from the center of the falloff curve for k_2 to allow for a safe determination of $F_{cent,2}$. Therefore, for simplicity, we identify $F_{cent,2}$ with $F_{cent,1}$. We emphasize that this needs not be true. Modifications of $F_{cent,2}$ may become necessary when measurements of k_2/k_1 at pressures near 10 bar and 298 K are also available. On the other hand, this uncertainty practically does not influence the determination of $F_{cent,1}$, which is close to F_{cent} from eq 2.5. Combining the data for $k = k_1 + k_2$ from Figure 1 and for k_2/k_1 from Figure 3, a fine-tuning of the parameters for $k_{2,0}$ and $k_{2,\infty}$ can be performed. It turns out that a simultaneous fit of the results shown in Figures 1 and 3 is very sensitive to the parameter choice. The best agreement with the experiments was found when the representation of the falloff curves, with broadening factors $F_1(x)$ and $F_2(x)$ fixed to

$$F_{cent,2} \approx F_{cent,1} = 0.41 \quad (3.1)$$

dx.doi.org/10.1021/jp212095n | J. Phys. Chem. A 2012, 116, 6387−6393

was made using eq 2.2 with the limiting rate constants

$$k_{1,0} = [N_2]3.2 \times 10^{-30}\ \text{cm}^6\ \text{molecule}^{-2}\ \text{s}^{-1} \quad (3.2)$$

$$k_{2,0} = [N_2]1.0 \times 10^{-31}\ \text{cm}^6\ \text{molecule}^{-2}\ \text{s}^{-1} \quad (3.3)$$

$$k_{1,\infty} = 2.7 \times 10^{-11}\ \text{cm}^3\ \text{molecule}^{-1}\ \text{s}^{-1} \quad (3.4)$$

$$k_{2,\infty} = 4.8 \times 10^{-11}\ \text{cm}^3\ \text{molecule}^{-1}\ \text{s}^{-1} \quad (3.5)$$

Figure 4 compares the corresponding falloff curve of $k = k_1 + k_2$ with the experimental data. The representation now

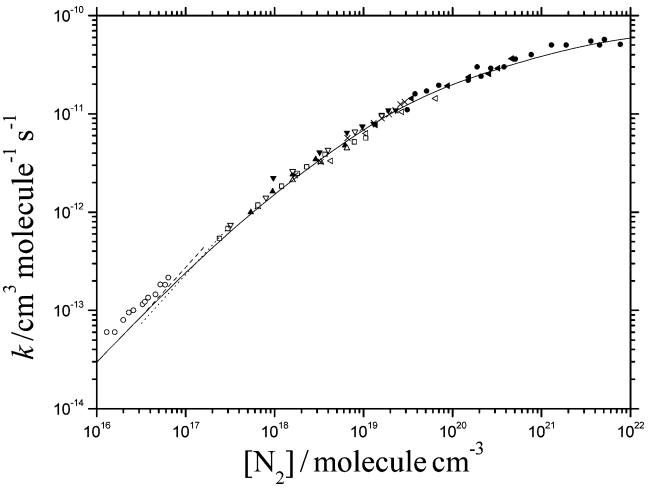

Figure 4. Comparison of experimental data for $k = k_1 + k_2$ with k from single-channel modelings of k_1 and k_2 (T = 298 K; full line = modeling as in Figure 3, experimental data points as in Figure 1).

looks even slightly better than that of Figure 1, in particular near $[N_2] = 10^{20}$ molecules cm^{-3} where the curve of the sum $k_1 + k_2$ slightly differs from the curve obtained with a single-reaction falloff curve. Figure 3 includes the modeled ratio k_2/k_1. The agreement with the experiment does not look perfect near $[N_2] = 7 \times 10^{18}$ molecules cm^{-3}. However, a modification of the parameters would deteriorate the joint agreement obtained in Figures 3 and 4. Therefore, the parameter choice given above appears to be the optimum obtainable at present.

The present work was not intended to assess the accuracy of the experimental data and the data representation. It relied on the average of the experimental data for 300 K and 2 Torr from refs 29 and 30, being close to k_0, the high pressure measurements of ref 9 extrapolated to k_∞, and the falloff representation with eq 2.2. As these three input elements still may be disputable, an assessment of the data representation appears premature. The accuracy of the experimental data near 1 bar has been discussed in detail in ref 4 and needs not be repeated here. However, the data representation of the present work extends over a much wider pressure range than considered in ref 4 and, therefore, is expected to provide more realistic limiting rate constants and center broadening factors.

4. TEMPERATURE DEPENDENCE OF FALLOFF CURVES

The analysis of sets of modeled falloff curves in ref 22 shows an increase of F_{cent}^{sc} from about 0.46 at 200 K to 0.64 at 1400 K. At the same time F_{cent}^{wc} according to eq 1.9 decreases with decreasing β_c until it levels off around a value[22] of 0.65. The two effects almost compensate each other such that, for M = N_2, tentatively one may neglect a temperature dependence of $F_{cent} = F_{cent}^{sc}F_{cent}^{wc}$ and keep it at its room temperature value 0.41. We note that this value agrees with the value predicted within the simplified theoretical treatment of the reaction in ref 15.

Theoretical estimates of the high pressure rate constant from refs 15−19 suggest that there is only a small temperature dependence of k_∞ between 200 and 400 K whereas $m \approx 0.6$ in eq 1.11 was predicted over the larger temperature range between 200 and 1400 K. In this situation we tentatively use $m = 0$ for our representation of the experiments. On the other hand, k_0 as usual has a marked negative temperature coefficient. The theoretical analysis of k_0 in ref 15, with only a weak temperature dependence of the total energy $\langle\Delta E\rangle$ transferred per collision, led to modeled temperature coefficients with n of the order of −3. The comparison with the experiments shown in Figure 6 led to $n = 4.5$ between 220 and 300 K and $n = 3.0$ between 300 and 430 K.

Extending eq 2.2 with temperature independent $F_{cent} = 0.41$, $m = 0$, and the fitted n to other temperatures, one obtains the ratio k_2/k_1 and falloff curves for $k = k_1 + k_2$ at 220 and 430 K such as shown in Figures 5 and 6. The high pressure

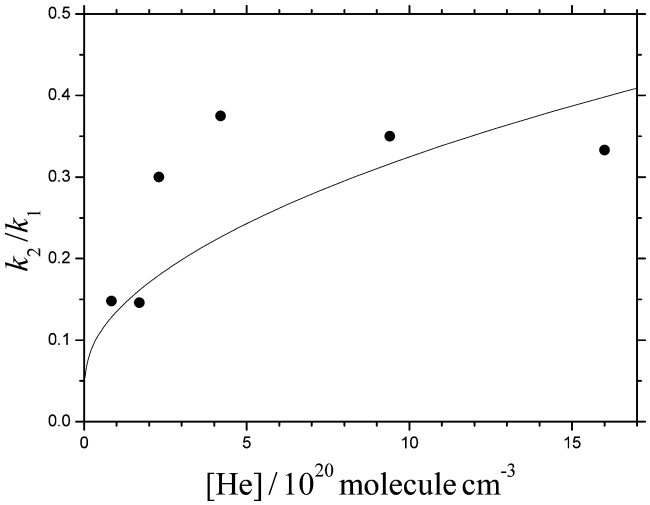

Figure 5. Comparison of experimental data for k_2/k_1 with k_2/k_1 from single-channel modelings for k_1 and k_2 (T = 430 K; full line = modeling with asymmetric falloff broadening factors of eq 2.2 using the parameters $F_{cent,1} = F_{cent,2} = 0.41$, $k_{1,0} = [He]7.1 \times 10^{-31}$ cm^6 molecule^{-2} s^{-1}, $k_{2,0} = [He]2.2 \times 10^{-32}$ cm^6 molecule^{-2} s^{-1}, $k_{1,\infty} = 2.7 \times 10^{-11}$ cm^3 molecule^{-1} s^{-1}, and $k_{2,\infty} = 4.8 \times 10^{-11}$ cm^3 molecule^{-1} s^{-1}; $k_{1,0}$ and $k_{2,0}$ proportional to $T^{-3.0}$ between 300 and 430 K; experimental points from ref 5).

measurements from ref 5 at 430 K in the bath gas He, after scaling [He] to [N_2] with the same factor of 0.64 as above are well reproduced. Extending the falloff calculations to 1400 K, where dissociation experiments in the bath gas Ar have been performed, one notes that the experiments were conducted under conditions very near the low pressure limit. Dissociation and recombination rate constants in the low pressure limit between 200 and 1400 K can be combined by using the equilibrium constant. This analysis has been performed within the simplified theoretical model of ref 15. The data were shown to be consistent with each other when only a weak temperature dependence of the average energy transferred per collision $\langle\Delta E\rangle$ was assumed. As this corresponds to the usual behavior of

dx.doi.org/10.1021/jp212095n | J. Phys. Chem. A 2012, 116, 6387−6393

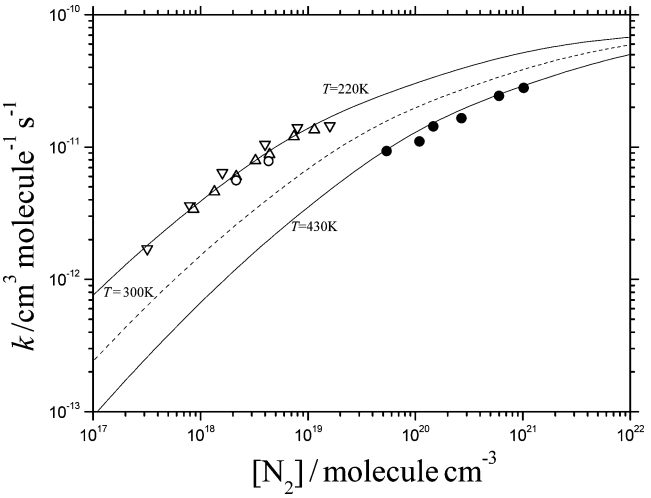

Figure 6. Comparison of experimental data for $k = k_1 + k_2$ with k from single-channel modelings of k_1 and k_2 (dashed line for T = 300 K from Figure 4, experimental points for 300 K omitted here, but given in Figures 1, 2, and 4; full line for 430 K = modeling as in Figure 5 but converted from M = He to N_2 with scaling factor 0.64; see text; experimental points from ref 5 (●); full line for 220 K = modeling with $F_{cent,1} = F_{cent,2} = 0.41$, $k_{1,0} = [N_2]12.8 \times 10^{-30}$ cm^6 molecule^{-2} s^{-1}, $k_{2,0} = [N_2]4.0 \times 10^{-31}$ cm^6 molecule^{-2} s^{-1}, experimental points from ref 23 (▽), ref 30 (△), and ref 34 (○); $k_{1,0}$ and $k_{2,0}$ proportional to $T^{-3.0}$ between 300 and 430 K and proportional to $T^{-4.5}$ between 220 and 300 K; see text).

$\langle \Delta E \rangle$ in low pressure dissociation and recombination reactions, the data indeed look consistent.

5. DISCUSSION

The present representation of experimental results for $k = k_1 + k_2$ in terms of the falloff expressions from ref 22 with asymmetric broadening factors shows excellent agreement even in the fine details and over the large pressure range 1 Torr to 330 bar of N_2 (near 300 K). It was shown that the experiments lead to a center broadening factor close to $F_{cent} \approx 0.41$. This clearly is in contrast to the NASA/JPL policy of fixing F_{cent} to a value of 0.6. Theoretical calculations of F_{cent} in ref 15 agreed with the experimental F_{cent} under the condition that weak collision broadening was also accounted for. The experimental ratio k_2/k_1 at 298 K from ref 4 over the range 100–760 Torr and from ref 5 over the range 5–90 bar at 430 K could be reproduced as well, however, within the larger experimental uncertainties.

The use of the falloff expressions from ref 22 with unsymmetric broadening factors removes some discrepancies observed in ref 9 between high pressure measurements and modeling with symmetric broadening factors in the falloff expressions (Figure 6 of ref 9). The use of $F_{cent} \approx 0.41$ instead of values near $F_{cent} = 0.6$ also leads to larger k_∞ than fitted in ref 9, k_∞ now approaching k_{13} from ref 11.

In summary, falloff curves in N_2 over the range 220–430 K can very well be fitted with the parameters

$$F_{cent,1} \approx F_{cent,2} \approx 0.41 \quad (5.1)$$

$$k_{1,0} = [N_2](T/300\text{K})^{-n} 3.2 \times 10^{-30} \text{ cm}^6 \text{ molecule}^{-2} \text{ s}^{-1} \quad (5.2)$$

$$k_{2,0} = [N_2](T/300\text{K})^{-n} 1.0 \times 10^{-31} \text{ cm}^6 \text{ molecule}^{-2} \text{ s}^{-1} \quad (5.3)$$

$$k_{1,\infty} = 2.7 \times 10^{-11} \text{ cm}^3 \text{ molecule}^{-1} \text{ s}^{-1} \quad (5.4)$$

$$k_{2,\infty} = 4.8 \times 10^{-11} \text{ cm}^3 \text{ molecule}^{-1} \text{ s}^{-1} \quad (5.5)$$

where $n \approx 4.5$ between 220 and 300 K and $n \approx 3$ between 300 and 430 K, and the asymmetric broadening factor of eq 2.2 is used. When the conventional falloff expression of eqs 1.3–1.9 with symmetric broadening factors is used with the same parameters, slightly larger deviations from the experiments in the high pressure range are obtained. These deviations are much less pronounced near the center of the falloff curve such that eqs 1.3–1.9 appear sufficient for atmospheric modeling. However, in this case, the parameters of eqs 5.4 and 5.5 have to be changed to effective values of

$$k^*_{1,\infty} = 3.0 \times 10^{-11} \text{ cm}^3 \text{ molecule}^{-1} \text{ s}^{-1} \quad (5.6)$$

$$k^*_{2,\infty} = 3.5 \times 10^{-11} \text{ cm}^3 \text{ molecule}^{-1} \text{ s}^{-1} \quad (5.7)$$

which are slightly different from the values obtained with asymmetric broadening factors.

AUTHOR INFORMATION

Notes

The authors declare no competing financial interest.

ACKNOWLEDGMENTS

The author acknowledges A. R. Ravishankara's eminent contributions to atmospheric chemical kinetics. Extensive discussion of this work with D. M. Golden has been most helpful as was communication with T. J. Wallington.

REFERENCES

(1) Sander, S. P.; Abbat, J.; Barker, J. R.; Burkholder, J. B.; Friedl, R. R.; Golden, D. M.; Huie, R. E.; Kolb, C. E.; Kurylo, M. J.; Moortgat, G. K. *JPL Publication 10-6*; Jet Propulsion Laboratory: Pasadena, CA, 2011; http://jpldataeval.jpl.nasa.gov.

(2) Atkinson, R.; Baulch, D. L.; Cox, R. A.; Crowley, J. N.; Hampson, R. G.; Jenkin, M. E.; Rossi, M. J.; Troe, J. *Atmos. Chem. Phys.* **2004**, *4*, 1461–1738. Atkinson, R.; Baulch, D. L.; Cox, R. A.; Crowley, J. N.; Hampson, R. F.; Hynes, R. G.; Jenkin, M. E.; Rossi, M. J.; Troe, J.; Wallington, T. J. *Atmos. Chem. Phys.* **2008**, *8*, 4141–4496.

(3) Troe, J. *J. Phys. Chem.* **1979**, *83*, 114–126.

(4) Mollner, A. K.; Valluvadasan, S.; Feng, K.; Sprague, M. K.; Okumura, M.; Milligan, D. B.; Bloss, W. J.; Sander, S. P.; Martien, P. T.; Harley, R. A.; McCoy, A. B.; Carter, W. P. L. *Science* **2010**, *330*, 646–649.

(5) Hippler, H.; Nasterlack, S.; Striebel, F. *Phys. Chem. Chem. Phys.* **2002**, *4*, 2959–2964.

(6) Harrison, H.; Johnston, H. S.; Hardwick, E. R. *J. Am. Chem. Soc.* **1962**, *84*, 2478–2482.

(7) Glänzer, K.; Troe, J. *Ber. Bunsen-Ges. Phys. Chem.* **1974**, *78*, 71–76.

(8) Gershenzon, Y. M.; Dement'ev, A. P.; Nalbandyan, A. B. *Kinet. Catal.* **1979**, *20*, 461–465.

(9) Hippler, H.; Krasteva, N.; Nasterlack, S.; Striebel, F. *J. Phys. Chem. A* **2006**, *110*, 6781–6788.

(10) Smith, I. W. M.; Williams, M. D. *J. Chem. Soc., Faraday Trans. II* **1985**, *81*, 1849–1860.

(11) D'Ottone, L.; Campuzano-Jost, P.; Bauer, D.; Hynes, A. J. *J. Phys. Chem. A* **2001**, *105*, 10538–10543.

(12) Chakraborty, D.; Park, J.; Lin, M. C. *Chem. Phys.* **1998**, *231*, 39−49.
(13) Golden, D. M.; Smith, G. P. *J. Phys. Chem. A* **2000**, *104*, 3991−3997.
(14) Matheu, D. M.; Green, W. H. *Int. J. Chem. Kinet.* **2000**, *32*, 245−262.
(15) Troe, J. *Int. J. Chem. Kinet.* **2001**, *33*, 878−889.
(16) Golden, D. M.; Barker, J.; Lohr, K. *J. Phys. Chem. A* **2003**, *50*, 11057−11071.
(17) Zhu, R. S.; Lin, M. C. *J. Chem. Phys.* **2003**, *119*, 10667−10677.
(18) Williams, C. F.; Pogrebnya, S. K.; Clary, D. C. *J. Chem. Phys.* **2007**, *126*, 154321−1−8.
(19) Cobos, C. J. *React. Kinet. Catal. Lett.* **2003**, *79*, 263−269.
(20) Troe, J. *Ber. Bunsen-Ges. Phys. Chem.* **1983**, *87*, 161−169.
(21) Gilbert, R. G.; Luther, K.; Troe, J. *Ber. Bunsen-Ges. Phys. Chem.* **1983**, *87*, 169−177.
(22) Troe, J.; Ushakov, V. G. *J. Chem. Phys.* **2011**, *135*, 054304−1−10.
(23) Anastasi, C.; Smith, I. W. M. *J. Chem. Soc., Faraday Trans. II* **1976**, *72*, 1459−1468.
(24) Robertshaw, J. S.; Smith, I. W. M. *J. Phys. Chem.* **1982**, *86*, 785−790.
(25) Wine, P. H.; Kreutter, N. M.; Ravishankara, A. R. *J. Phys. Chem.* **1979**, *83*, 3191−3195.
(26) Donahue, N. M.; Dubey, M. K.; Mohrschladt, R.; Demerjian, K. L.; Anderson, J. G. *J. Geophys. Res. Atmos.* **1997**, *102*, 6159−6168.
(27) Howard, C. J.; Evenson, K. M. *J. Chem. Phys.* **1974**, *61*, 1943−1952.
(28) Anderson, J. G.; Margitan, J. J.; Kaufman, F. *J. Chem. Phys.* **1974**, *60*, 3310−3317.
(29) Burrows, J. P.; Wallington, T. J.; Wayne, R. P. *J. Chem. Soc., Faraday Trans. 2* **1983**, *79*, 111−122.
(30) Brown, S. S.; Talukdar, R. K.; Ravishankara, A. R. *Chem. Phys. Lett.* **1999**, *299*, 277−284.
(31) Nizkorodov, S. A.; Wennberg, O. *J. Phys. Chem. A* **2002**, *106*, 855−859.
(32) Bean, B. D.; Mollner, A. K.; Nizkorodov, S. A.; Nair, G.; Okumura, M.; Sander, S. P.; Peterson, K. A.; Francisco, J. S. *J. Phys. Chem. A* **2003**, *107*, 6974−6985.
(33) D'Ottone, L.; Bauer, D.; Campuzano-Jost, P.; Fardy, M.; Hynes, A. J. *Faraday Discuss.* **2005**, *130*, 111−123.
(34) Dransfield, T. J.; Perkins, K. K.; Donahue, N. M.; Anderson, J. G.; Sprengnether, M. M.; Demerjian, K. L. *Geophys. Res. Lett.* **1999**, *26*, 687−690.